



Increase lattice Boltzmann method ability to simulate slip flow regimes with dispersed CNTs nanoadditives inside

Develop a model to include buoyancy forces in distribution functions of LBM for slip velocity

Masoud Mozaffari¹ · Arash Karimipour¹ · Annunziata D’Orazio²

Received: 23 June 2018 / Accepted: 11 November 2018 / Published online: 23 November 2018
© Akadémiai Kiadó, Budapest, Hungary 2018

Abstract

In this study, the mixed convection of flow in a microchannel containing nanofluid is simulated by the Lattice Boltzmann Method. The water/functionalized multi-wall carbon nanotubes nanofluid is selected as the working fluid. The cold nanofluid passes through the warm walls of the microchannel to cool them down. The buoyancy forces caused by the mass of the nanofluid change the hydrodynamic properties of the flow. Accordingly, the gravitational term is included as an external force in the Boltzmann equation and Boltzmann’s hydrodynamic and thermal equations are rewritten under new conditions. The flow analysis is performed for different values of slip coefficient and Grashof number. The results are expressed in terms of velocity and temperature profiles, contours of streamlines and isotherms beside the slip velocity and temperature jump diagrams. It is observed that the effect of buoyancy force changes the motion properties of the flow in the input region and increases the hydrodynamic input length of flow. These changes are particularly evident at higher values of Grashof numbers and create a rounded circle in the opposite direction of the flow at the microchannel input. The negative slip velocity caused by the vortex resulted in a temperature jump at the input flow region.

Keywords Lattice Boltzmann method · Slip velocity · Temperature jump

List of symbols

c Microscopic velocity
 D_H Hydraulic diameter (m)
 f Hydrodynamic distribution function
 g Thermal distribution function
 G Buoyancy force
 Gr Grashof number
 h Height of microchannel (m)
 l Length of microchannel (m)
 B Dimensionless slip coefficient
 Pr Prandtl number
 Re Reynolds number

U Horizontal dimensionless velocity
 U_s Dimensionless slip velocity
 V Vertical dimensionless velocity
 X Dimensionless horizontal Cartesian coordinates
 Y Dimensionless vertical Cartesian coordinates

Greek symbols

θ Dimensionless profiles of temperature
 θ_s Dimensionless temperature jump
 ν Kinematic viscosity ($m^2 s^{-1}$)

Introduction

Convection heat transfer is one of the most important and most widely used industrial topics which has always been studied by the energy due to the optimization of energy efficiency. On the other hand, the global development of research on microelectromechanical (MEMS) and nano-electromechanical (NEMS) systems suggests the growth of investment and the use of this technology in a variety of

✉ Arash Karimipour
arashkarimipour@gmail.com;
arash.karimipour@pmc.iaun.ac.ir

¹ Department of Mechanical Engineering, Najafabad Branch, Islamic Azad University, Najafabad, Iran

² Dipartimento di Ingegneria Astronautica, Elettrica ed Energetica, Sapienza Università di Roma, Via Eudossiana 18, 00184 Rome, Italy

areas, including the automotive industry, medicine, and electronic applications in telecommunication and defense systems. The abundant capabilities of this field have accelerated innovation and increased patents in the field of microprocessors. Therefore, the use of lattice Boltzmann method which is appropriate for flow simulation in microscopic dimensions is increasing [1].

So far various numerical methods have been introduced for analyzing and simulating heat transfer. Generally, the fluid flow can be in two ways. The first method involves fluid continuum in which macroscopic equations are presented. The classic Navier–Stokes (NS) equations [2] contain the same method. The second method consists of particle-based methods the performance of which is based on the action and reaction between fluid particles [3]. This method has a large volume and is not suitable for use in macroscopic dimensions. The lattice Boltzmann method (LBM) is one of the particle-based methods with lower computational cost than other particle-based methods such as the molecular dynamics (MD) method and direct simulation of Monte Carlo (DSMC) [4–6]. Therefore, many researchers have used this method [7, 8]. The lattice Boltzmann method is a new way for simulating compressible viscous flows and has the most application range in a variety of fluid flow regimes. This method can well be used to simulate convective flow and heat transfer in multiphase, liquid–gas systems in microscopic dimensions [9–11]. In LBM by averaging the microscopic particles' properties, it is possible to gain macroscopic quantities of the flow and provide the mass and momentum conservation equations [12–15]. The performance of this method involves the steps of collision at a location and diffusion within the range of fluid flow [16]. The BGK operator [17] is used to express the particles' collision where the Boltzmann equation has a proper accuracy and has a good convergence in the thermal lattice Boltzmann which is also based on internal energy of the fluid [18–21].

The desirability of this method has led to its increasing use in the studies conducted by the engineers and has made it more versatile in fluid flow simulations by providing different models [22–24]. Microstructure simulation using LBM and Langmuir slip model adoption by Chen et al. [25] is an example of it. He introduced the developed Langmuir slip model instead of Maxwell slip model that had a brighter physical image. Also, the relationship between the molecular slip coefficient and the macroscopic slip length in a Newtonian fluid proposed using LBM by Oldrich and Jan [26] is an alternative method for calculating the local shear rate for calculating the macroscopic slip length. Due to the wide application of LBM and the presentation of varied models, modified relationships are proposed to be applied in solving various problems including the introduction of a modified Richardson

number by Monfared et al. [27]. They used LBM to determine the thermal flux in a successive square cylinder with the constant thermal flux boundary condition in 2D mode. The results of their work showed that using the buoyancy force term in hydrodynamic and thermal equations creates a vortex phenomenon in the fluid flow and the amount of buoyancy force has a great effect on the start of the vortex and the lift and drag force. The LBM has a good accuracy in simulating irregular geometries and complicated boundary conditions [28, 29], and it has an optimal performance in the analysis of channels with curved walls [30]. Also, the simulation of the displacement of the fluid inside the chamber and the obstructed channels by LBM has been reported in many studies [31–34].

In recent years, various simulations have been performed in various conditions [35–88]. Also the analysis of the Couette and Poiseuille flow within a microchannel has been studied by LBM under various conditions using [39–41]. Gas flow analysis within microchannels is very important in engineering fields due to its diverse applications. Shu et al. [42] studied the gas flow inside the microchannel with the aid of the diffuse scattering boundary condition (DSBC) using LBM. In adapting his results, he was able to provide an acceptable mathematical model for simulating the flow of microchannels. Liu and colleagues studied the gas flow in a long microchannel using the LBM. He showed that LBM equation can describe the flow behavior of the fluid in the transient region. Then Yun and Rahman [44] studied the gas flow in the microchannel by means of LBM for a range of different Knudsen numbers with several comfort times. They examined the effect of the Knudsen layer on the gas flow rate for different Knudsen numbers.

The present study simulates the effect of buoyancy force on the flow components in the microchannel using LBM and simulates the effect of varying slip flow parameters such as Grashof number and slip coefficient on the hydrodynamic and thermal properties of the fluid flow.

Statement of the problem

In the present work, the mixed convection of heat transfer is investigated in microscopic dimensions. Here the water/functionalized multi-wall carbon nanotube (FMWCNT) nanofluid mixed convection is studied in a long 2-D microchannel under fixed wall temperature in slip flow regime and by using LBM. The force of mass as an external force influences the collision between fluid particles and the fluid flow causes mixed convection movements within the microchannel. The cold air flows into the microchannel and leaves it after cooling the walls, $T_w = 2T_c$. In parallel with this flow, gravity also changes

the velocity components in the direction of perpendicular to the flow and by creating a vertical temperature gradient creates free convection. Since the Reynolds number is small in the microchannel, the presumed value for Reynolds is equal to $Re = 0.01$ and $Pr = 4.42$ which represents the mass fraction of 0.0025 of *FMWCNT* in water [45].

The effect of gravity on the formation of mixed convection is investigated on different flow parameters for $B = 0.1, 0.01$ and 0.001 and $Gr = 1, 10$ and 100 . The flow is in a two-dimensional microchannel with an aspect ratio of $AR = 30$ and hot walls. Because of the length of the microchannel after the input, the conditions are fully developed for velocity and temperature (See Fig. 1).

Assumptions

The microflows are classified based on Knudsen number and have a certain limit for different flow regimes. λ is the mean molecular free path and D_h is the hydraulic diameter (characteristic length):

$$Kn = \frac{\lambda}{D_H} \tag{1}$$

$$Kn = \sqrt{\frac{\pi k Ma}{2 Re}} \tag{2}$$

The sound speed is $C_s = (kRT)^{0.5}$ and Reynolds and Mach numbers are $Re = UL/\nu$ and $Ma = U/C_s$, k also represents the specific heat ratio ($k = c_p/c_v$). A computer code is developed in FORTRAN language to simulate the fluid flow and heat transfer. To have appropriate convergence through the solvation process, the compressibility error of LBM should be small. The compressibility error of density variation is proportional to Ma^2 . Hence it will be negligible for the low value of Mach number which is chosen as 0.1 through the present using code.

Moreover, the hydrodynamic and thermal relaxation times are considered as $\tau_f = \sqrt{6/(\pi k)}D_HKn$ and $\tau_g = \tau_f/Pr$, respectively [22]. It should mentioned that the expression of Knudsen number is not usually applied for the *liquid microflows*. As a result, the dimensionless slip coefficient of “ $B = (\text{Slip coefficient})/(\text{Characteristic$

length) = 0.1, 0.01 and 0.001” is used instead of “ $Kn = 0.1, 0.01$ and 0.001” in the following parts of the present work which represents the same theoretical and physical concepts [52].

Equations

Boltzmann equation

The lattice Boltzmann equation obtained by Lattice Gas Automata developed by Frisch et al. The performance of this model consists of the collision processes in one place and diffusion in the fluid range in a time step. If the diffusion function f denotes the statistical description of the probability of the presence of particles in the place and time x and t , at a particle velocity (microscopic) of c , the macroscopic quantities of density, velocity vector, internal energy, and heat flux can be calculated:

$$\rho(x, t) = \int f(x, c, t)dc \tag{3}$$

$$\rho u(x, t) = \int c f(x, c, t)dc \tag{4}$$

$$\rho e(x, t) = \int c_o^2 f(x, c, t)dc \tag{5}$$

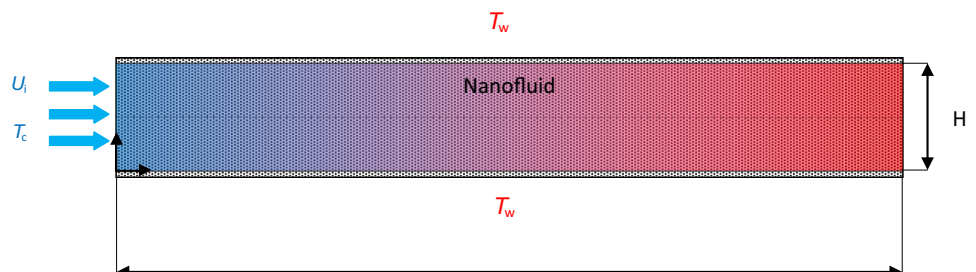
$$q(x, t) = \frac{1}{2} \int c_o(c_o \cdot c_o) f(x, c, t)dc \tag{6}$$

An external force F on the unit gas molecule mass leads to a change in the particle velocity and its displacement. In this case the distribution function f for particles at time t , in the space interval x , has a velocity between c and $c + dc$. Thus the Boltzmann equation is written as follows:

$$f(x + cdt, c + Fdt, t + dt)dxdc - f(x, c, t)dxdc = 0 \tag{7}$$

By introducing an appropriate operator for the collision term, it is possible to achieve the distribution of particles after the collision and diffuse the effect of new alignment on the entire flow range.

Fig. 1 Microchannel formation



$$f(x + cdt, c + Fdt, t + dt) dxdc - f(x, c, t) = \Omega(f) dxdc dt \tag{8}$$

Thus

$$\frac{\partial f}{\partial t} + \frac{\partial f}{\partial x} \cdot c + \frac{F}{m} \cdot \frac{\partial f}{\partial c} = \Omega \tag{9}$$

If the external force is ignored, the Boltzmann equation is written as follows:

$$\frac{\partial f}{\partial t} + c_o \nabla f = \Omega \tag{10}$$

BGK approximation

The collision operator represents the rate of change in the distribution function. These changes occur between the initial and final modes of the distribution function due to collision between particles. Because of the complexity of Boltzmann equation solution, so far various models have presented to solve it; a simple and popular model that is introduced for the collision operator is the BGK model:

$$\Omega = -\omega (f^{eq} - f) \tag{11}$$

f^{eq} is the local equilibrium distribution function; ω is the collision frequency and τ is the coefficient of comfort that are inversely correlated ($\omega = \frac{1}{\tau}$) By introducing the BGK approximation, the Boltzmann equation is expressed as follows:

$$\frac{\partial f}{\partial t} + c_i \frac{\partial f}{\partial x} + \frac{F_i}{m} \cdot \frac{\partial f}{\partial c_i} = \omega (f^{eq} - f) \tag{12}$$

Boltzmann equation with BGK approximation without the external force F is rewritten as follows:

$$\frac{\partial f}{\partial t} + c_i \frac{\partial f}{\partial x_i} = \omega (f^{eq} - f) \tag{13}$$

Hydrodynamic lattice Boltzmann relations

The analytic solution of Boltzmann equation is difficult even with the BGK collision operator which is a simple and suitable model. Therefore, this equation must be discretized and solve approximately. To facilitate solution, discretization is done on the velocity domain using a symmetric network at certain velocities.

In this case, the distribution function is discretized that α represents the direction of the discretization rate on the lattice and, as mentioned, the macroscopic properties are obtained by summing up the microscopic properties and the laws of conservation of mass, momentum and energy are calculated as follows:

$$\begin{aligned} \rho &= \sum_{\alpha=0}^b f_{\alpha} \\ \rho u &= \sum_{\alpha=1}^b e_{\alpha} f_{\alpha} \\ \rho e &= \sum_{\alpha=1}^b c_{o\alpha}^2 f_{\alpha} \end{aligned} \tag{14}$$

Finally, using Eq. (12) and applying the Boussinesq approximation (all fluid characteristics except density are constant in the buoyancy force term) and considering the effects of the mass force on the fluid flow, the Boltzmann discrete motion equation is written as follows:

$$\begin{aligned} f_{\alpha}(x + e_{\alpha} \Delta t, t + \Delta t) - f_{\alpha}(x, t) &= \frac{-\Delta t}{\tau_f + 0.5 \Delta t} [f_{\alpha}(x, t) - f_{\alpha}^{eq}(x, t)] \\ &+ \left(\frac{\Delta t \tau_f}{\tau_f + 0.5 \Delta t} \frac{3G(e_{\alpha y} - V)}{C^2} f^{eq} \right) \end{aligned} \tag{15}$$

where β coefficient of volumetric expansion and G is the buoyancy force per unit of mass defined as $G = \beta g(T - \bar{T})$ that g is the force of gravity. In this relation, the last right term denotes the collision of particles under the influence of the gravitational buoyancy force.

Equilibrium distribution in the BGK model

The BGK approximation represents the density distribution function in terms of the equilibrium distribution function and no macroscopic velocity exists in the equilibrium distribution function because it is considered constant. Therefore, the values of motion equilibrium distribution function values are calculated as follows:

$$f_{\alpha}^{eq} = \omega_{\alpha} \rho \left[1 + \frac{3(e_{\alpha} \cdot u)}{c^2} + \frac{9(e_{\alpha} \cdot u)^2}{2c^4} - \frac{3u^2}{2c^2} \right] \tag{16}$$

In the D_2Q_9 model (Fig. 2), the microscopic velocity vectors of the lattice particles are calculated as follows. Mass functions are also in the form of $\omega_{\alpha=0} = \frac{4}{9}$, $\omega_{\alpha} = \frac{1}{9}$ for $\alpha = 1, 2, 3, 4$ and $\omega_{\alpha} = \frac{1}{36}$ for $\alpha = 5, 6, 7, 8$.

$$\begin{aligned} e_{\alpha} &= \left(\cos \frac{\alpha - 1}{2} \pi, \sin \frac{\alpha - 1}{2} \pi \right) c, \quad \alpha = 1, 2, 3, 4 \\ e_{\alpha} &= \sqrt{2} \left(\cos \left[\frac{\alpha - 5}{2} \pi + \frac{\pi}{4} \right], \sin \left[\frac{\alpha - 5}{2} \pi + \frac{\pi}{4} \right] \right) c, \quad \alpha = 5, 6, 7, 8 \\ e_0 &= (0, 0) \end{aligned} \tag{17}$$

As already mentioned, the flow range can be calculated by macroscopic quantities. The laws of conservation of mass, momentum and energy are as follows:

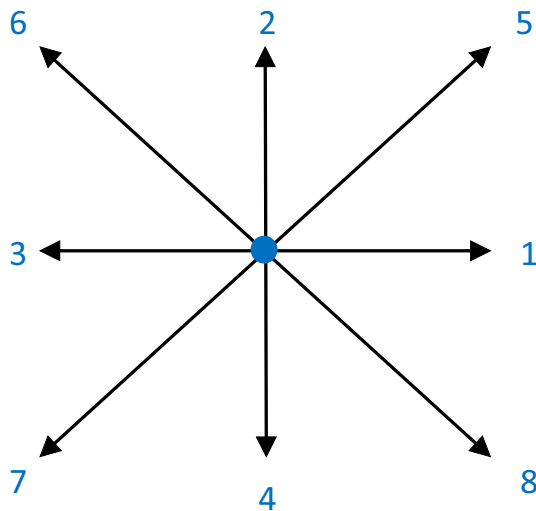


Fig. 2 D_2Q_9 lattice

$$\rho = \sum_{\alpha} f_{\alpha} \tag{18}$$

$$u = (1/\rho) \sum_{\alpha} f_{\alpha} e_{\alpha x} \tag{19}$$

$$v = (1/\rho) \sum_{\alpha} f_{\alpha} e_{\alpha y} + \frac{\Delta t}{2} G \tag{20}$$

The discretized distribution function in the presence of buoyancy force is as follows:

$$f_{\alpha} = \frac{\tau_f f_{\alpha} + 0.5\Delta t f_{\alpha}^{eq}}{\tau_f + 0.5\Delta t} + \left(\frac{0.5\Delta t \tau_f}{\tau_f + 0.5\Delta t} \frac{3G(e_{\alpha y} - V)}{c^2} f_{\alpha}^{eq} \right) \tag{21}$$

Thermal lattice Boltzmann relations

The optimal performance of lattice Boltzmann in solving the mixed convection problems and its proper application in simulating multi-phase flows and different geometries lead to its increased application.

In the hydraulic analysis of the flow through the lattice Boltzmann, the second-order accuracy is used to satisfy the laws of conservation and the equilibrium function versus velocity will be of the second order. Thus the thermal energy distributed function model by He et al. [18] is used in the simulation of heat transfer in the LBM where a separate distribution function, g , is used to simulate the temperature field. This model is applicable to complex geometries and boundary conditions.

The BGK thermal lattice Boltzmann model based on internal energy is described as follows over a process similar to discretization of hydrodynamic lattice

Boltzmann with BGK approximation. Thermal lattice Boltzmann equation which includes the collision and diffusion:

$$\begin{aligned} &\tilde{g}_{\alpha}(x + e_{\alpha}\Delta t, t + \Delta t) - \tilde{g}_{\alpha}(x, t) \\ &= - \frac{\Delta t}{\tau_g + 0.5\Delta t} [\tilde{g}_{\alpha}(x, t) - g_{\alpha}^{eq}(x, t)] \\ &\quad - \frac{\tau_g \Delta t}{\tau_g + 0.5\Delta t} f_{\alpha}(x, t) Z_{\alpha}(x, t) \end{aligned} \tag{22}$$

That

$$\tilde{g}_{\alpha} = g_{\alpha} - \frac{\Delta t}{2\tau_g} (g_{\alpha} - g_{\alpha}^{eq}) + \frac{\Delta t}{2} f_{\alpha} Z_{\alpha} \tag{23}$$

The heat loss due to viscosity and condensation in the equation above are as follows:

$$Z_{\alpha} = [e_{\alpha} - u(x, t)] \cdot [u(x \cdot e_{\alpha}\Delta t, t + \Delta t) - u(x, t)]/\Delta t \tag{24}$$

Discretized lattice Boltzmann equation:

$$\begin{aligned} g_0^{eq} &= - \frac{4}{9} \left[\frac{3\rho e u^2 + v^2}{2c^2} \right] \\ g_{\alpha}^{eq} &= \frac{1}{9} \rho e \left[1.5 + 1.5 \frac{e_{\alpha} \cdot u}{c^2} + 4.5 \frac{(e_{\alpha} \cdot u)^2}{c^4} - 1.5 \frac{u^2 + v^2}{c^2} \right], \\ &\quad \alpha = 1, 2, 3, 4 \\ g_{\alpha}^{eq} &= \frac{1}{9} \rho e \left[3 + 6 \frac{e_{\alpha} \cdot u}{c^2} + 4.5 \frac{(e_{\alpha} \cdot u)^2}{c^4} - 1.5 \frac{u^2 + v^2}{c^2} \right], \\ &\quad \alpha = 5, 6, 7, 8 \end{aligned} \tag{25}$$

$$\begin{aligned} \rho e &= \sum_{\alpha} \tilde{g}_{\alpha} - \frac{\Delta t}{2} \sum_{\alpha} f_{\alpha} Z_{\alpha} \\ q &= \left(\sum_{\alpha} e_{\alpha} \tilde{g}_{\alpha} - \rho e u - \frac{\Delta t}{2} \sum_{\alpha} e_{\alpha} f_{\alpha} Z_{\alpha} \right) \frac{\tau_g}{\tau_g + 0.5\Delta t} \end{aligned} \tag{26}$$

Boundary conditions

The application of boundary conditions in the LBM is very different from the methods of the Navier–Stokes equations and has a more complex process due to the use of the distribution function variable. In this method, boundary conditions affect the distribution functions and these effects are applied to the hydrodynamic and thermal properties of the flow indirectly. In lattice Boltzmann, the domain of the solution must be divided into lattices that distribution function particles are on each lattice. Some of these particles flow along the specified directions to the adjacent nodes.

Hydrodynamic boundary conditions

In the fluid flow in the microscopic dimensions, the fluid slips on the channel walls with a limited tangential velocity which causes the slip boundary condition on the walls to be applied. The directions of the velocities thrown by the fluid domain to the boundaries are considered as known quantities, and it is not necessary to calculate them on the boundary and their values are obtained from the previous stages of the collision and the previous diffusion of the fluid range. Here, the unknown distribution functions can be obtained using unbalanced return boundary condition [46]. In this model, the collision is performed on a node on the solid–fluid boundary and the distribution functions colliding with the wall are returned in a direction that is in line with equilibrium conditions. The left wall with distribution functions related to directions $\alpha = 1, 5$ and 8 is the missing quantities:

$$f_1 = f_3 + \frac{2}{3} \rho_{in} u_{in}$$

$$f_5 = f_7 + \frac{f_4 - f_2}{2} + \frac{1}{6} \rho_{in} u_{in} + \frac{1}{2} \rho_{in} V_{in} - \frac{\Delta t}{4} \rho_{in} G \tag{27}$$

$$f_8 = f_6 - \frac{f_4 - f_2}{2} + \frac{1}{6} \rho_{in} u_w - \frac{1}{2} \rho_{in} V_{in} + \frac{\Delta t}{4} \rho_{in} G$$

$$\tilde{f}_3 = \tilde{f}_1 - \frac{2}{3} \rho_{out} u_{out}$$

$$\tilde{f}_7 = \tilde{f}_5 - \frac{1}{2} (\tilde{f}_4 - \tilde{f}_2) - \frac{1}{6} \rho_{out} u_{out} - \frac{1}{2} \rho_{out} v_{out} + \frac{1}{4} \Delta t \rho_{out} G$$

$$\tilde{f}_6 = \tilde{f}_8 - \frac{1}{2} (\tilde{f}_4 - \tilde{f}_2) - \frac{1}{6} \rho_{out} u_{out} + \frac{1}{2} \rho_{out} v_{out} - \frac{1}{4} \Delta t \rho_{out} G \tag{28}$$

The upper and lower walls have different boundary condition because of the slip in the walls and here the Knudsen number is important. In this situation, fluid molecules located on the wall surface slip on it and cause a slip boundary condition in hydrodynamic problems. Slip velocity condition:

$$\Delta u_{wall} = u_{fluid(y \rightarrow wall)} - u_{wall} = \ell_S \frac{\partial u_{fluid}}{\partial y} \Big|_{wall} \tag{29}$$

Maxwell completes the above relation by introducing the tangential momentum accommodation coefficient

$$u_{slip} = u_s - u_{wall} = \frac{2 - \sigma}{\sigma} \lambda \frac{\partial u_S}{\partial n} \Big|_w + \frac{3}{4} \frac{\eta}{PT} \frac{\partial T}{\partial S} \Big|_w \tag{30}$$

In dimensionless form : $U_{slip} = B \frac{\partial U}{\partial n} \Big|_w$

where B represent the dimensionless slip coefficient. Slip velocity boundary condition in lattice model [47]:

$$\tilde{f}_4 = \tilde{f}_2$$

$$\tilde{f}_7 = r \tilde{f}_5 + (1 - r) \tilde{f}_6 \tag{31}$$

$$\tilde{f}_8 = r \tilde{f}_6 + (1 - r) \tilde{f}_5$$

$$\tilde{f}_2 = \tilde{f}_4$$

$$\tilde{f}_5 = r \tilde{f}_7 + (1 - r) \tilde{f}_8 \tag{32}$$

$$\tilde{f}_6 = r \tilde{f}_8 + (1 - r) \tilde{f}_7$$

where $r = 0.7$ is chosen as the matching coefficient.

Thermal boundary conditions

As mentioned before in a fluid flow in microscopic dimensions, the fluid slips on a channel wall with limited tangential velocity causing thermal jumps to occur in thermal problems. Here, the thermal boundary condition is applied using the model provided by He et al. [18] which has a proper function. In their model, the non-equilibrium return boundary condition by Zhu and He functions is used [48]. In the present study, the thermal boundary condition is constant temperature and insulated wall. D’Orazio et al. [49] applied He’s model and complete it by *GPTBC* model. In this model, the unknown thermal distribution functions are equalized with equilibrium distribution functions with reverse slip thermal energy:

$$\tilde{g}_5 = \frac{1}{12} \left[1.5 \Delta t \sum_{\alpha=1}^8 e_{\alpha x} f_{\alpha} Z_{\alpha} + 3(\tilde{g}_3 + \tilde{g}_6 + \tilde{g}_7) \right]$$

$$\tilde{g}_1 = \frac{1}{6} \left[1.5 \Delta t \sum_{\alpha=1}^8 e_{\alpha x} f_{\alpha} Z_{\alpha} + 3(\tilde{g}_3 + \tilde{g}_6 + \tilde{g}_7) \right] \tag{33}$$

$$\tilde{g}_8 = \frac{1}{12} \left[1.5 \Delta t \sum_{\alpha=1}^8 e_{\alpha x} f_{\alpha} Z_{\alpha} + 3(\tilde{g}_3 + \tilde{g}_6 + \tilde{g}_7) \right]$$

$$\tilde{g}_6 = \frac{1}{12} \left[-1.5 \Delta t \sum_{\alpha=1}^8 e_{\alpha x} f_{\alpha} Z_{\alpha} + 3(\tilde{g}_1 + \tilde{g}_5 + \tilde{g}_8) \right]$$

$$\tilde{g}_3 = \frac{1}{6} \left[-1.5 \Delta t \sum_{\alpha=1}^8 e_{\alpha x} f_{\alpha} Z_{\alpha} + 3(\tilde{g}_1 + \tilde{g}_5 + \tilde{g}_8) \right] \tag{34}$$

$$\tilde{g}_8 = \frac{1}{12} \left[-1.5 \Delta t \sum_{\alpha=1}^8 e_{\alpha x} f_{\alpha} Z_{\alpha} + 3(\tilde{g}_1 + \tilde{g}_5 + \tilde{g}_8) \right]$$

The unknown distribution functions of g on the lower and upper walls are as follows to simulate the temperature jump boundary condition:

$$\begin{aligned} \tilde{g}_2 &= \frac{3}{\rho e} g_2^{eq}(\rho_w, u_w, e_w)(g_7 + g_4 + g_8) \\ \tilde{g}_5 &= \frac{3}{\rho e} g_5^{eq}(\rho_w, u_w, e_w)(g_7 + g_4 + g_8) \end{aligned} \tag{35}$$

$$\begin{aligned} \tilde{g}_6 &= \frac{3}{\rho e} g_6^{eq}(\rho_w, u_w, e_w)(g_7 + g_4 + g_8) \\ \tilde{g}_4 &= \frac{3}{\rho e} g_2^{eq}(\rho_w, u_w, e_w)(g_2 + g_5 + g_6) \\ \tilde{g}_7 &= \frac{3}{\rho e} g_7^{eq}(\rho_w, u_w, e_w)(g_2 + g_5 + g_6) \end{aligned} \tag{36}$$

The velocity and temperature values are also calculated as dimensionless as follows:

$$U = u/u_i \tag{37}$$

$$\theta = T/T_c \tag{38}$$

The dimensional quantities of spatial coordinates x and y also become dimensionless as follows:

$$X = x/H \tag{39}$$

$$Y = y/H \tag{40}$$

It should be noted that $L/H = 30$. Therefore, for the dimensionless quantities of X and Y used in plotting the output charts and figures: $0 < Y < 1$ and $0 < X < 30$. The following equation is used for the Nusselt number [52].

$$Nu = \frac{k_{nf}}{k_f} \frac{D_H \frac{\partial T}{\partial y}_w}{T_w - T_{bulk}} \tag{41}$$

Validation

For implementation of the numerical solution of the problem algorithm, a computer code written in *FORTRAN* language is used. To verify the independence of the solution process to the number of point in the lattice, it is examined according to Table 1. The mean value of the Nusselt number, as well as the dimensionless values of the horizontal velocity U , the vertical velocity W , and the dimensionless temperature θ at $X = 1.5$ for three lattices 35×350 , 40×400 and 450×450 are shown. Due to the

Table 1 Checking the independence of the lattice in terms of the flow in the microchannel for $B = 0.01$ and $Re = 0.01$

	350 × 35	400 × 40	450 × 45
Nu	7.18	7.23	7.25
$C_f Re$	21.04	21.10	21.13

small difference between the lattices' results, 40×400 lattice is applied for further calculations.

In order to verify the performance validity of the code and the applied relations, the flow of fluid inside the microchannel is studied in the slip flow regime and then compressible fluid flow in the microchannel under different boundary conditions. In the first problem the results of the present study are compared with the results of Zhang et al. [15] in Fig. 3 for validating numerical solution for fluid flow properties. Using the LBM, they simulated gas flow in the slip flow regime within the microchannel. According to the above-mentioned figure, the dimensionless velocity profile of Zhang et al. for $Kn = 0.05$ and 0.1 shows a good consistency with the present work.

To evaluate the accuracy of the numerical solution in the heat transfer problems in microscopic dimensions, the results were compared with the results of Kavehpour et al. [23]. They modeled the compressible fluid flow in a microchannel under the boundary conditions of temperature and constant thermal flux using LBM. Figure 4 shows the comparison between dimensionless temperature profiles in the fluid flow for $Re = 0.01$ and $Kn = 0.01$ (similar to the present work). The results of comparison show an acceptable match.

In Table 2 the coefficient of friction amounts, $C_f Re$, and Knudsen number, Kn , are compared with those of Kavehpour et al. [23]. The accuracy of the performed simulation by comparing the results with past valid research indicates the high accuracy of the written computer code.

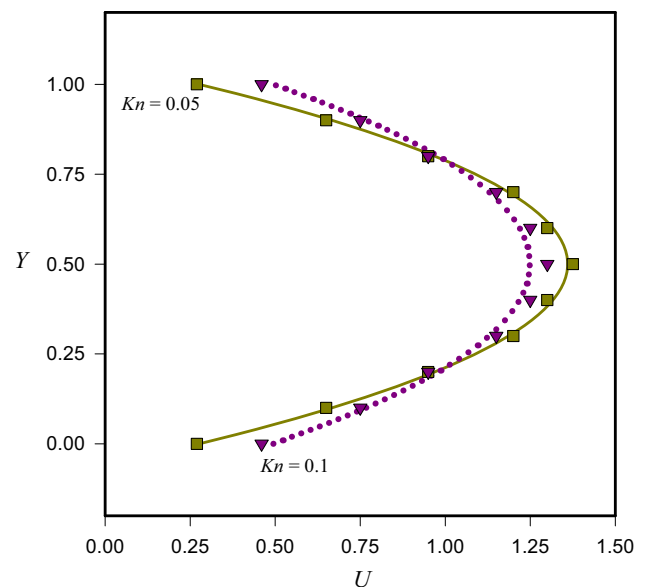


Fig. 3 Dimensionless velocity profiles (lines) with those of Zhang et al. [15] (symbols)

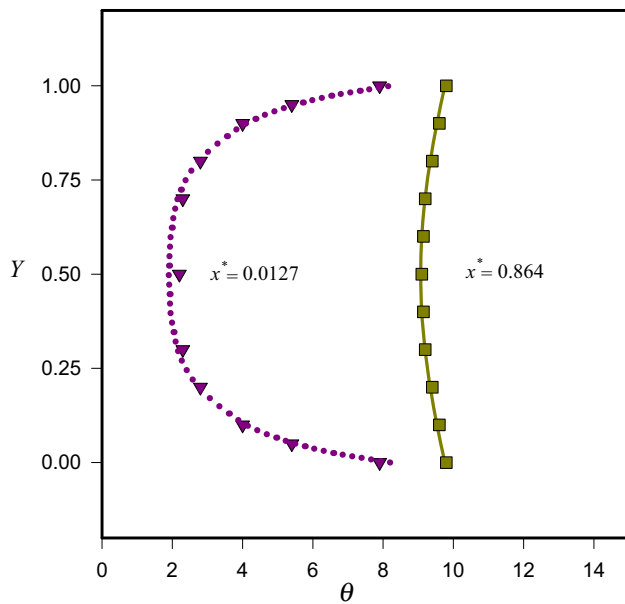


Fig. 4 Dimensionless temperature profiles of $\theta = T/T_i$ at various cross sections of microchannel for $Kn = 0.01$ (lines) with Kavehpour et al. [23] (symbols)

Results and discussion

The laminar flow of cold nanofluid in a microchannel at a constant heat flux for cooling the walls is examined in a two-dimensional mode using the LBM. The effect of gravity on the flow and mixed convection heat transfer in a microchannel for different values of $B = 0.001, 0.01$ and 0.1 are investigated. It should be noted that the Reynolds number is $Re = 0.01$. The effect of buoyancy force on free motion is applied by Boussinesq approximation. The water/functionalized multi-wall carbon nanotubes nanofluid (see Table 3) is considered as the working fluid with different Grashof numbers as $Gr = 1, 10$ and 100 . The Grashof number indicates the buoyancy to viscosity forces ratio and using $Gr = g\beta D_H^3(T_h - T_c)/\nu^2$ and constant values for viscosity are assumed at $\beta = 1/T$ and $g = 9.8 \text{ ms}^{-2}$.

Table 2 Validation of the coefficient of friction amounts and Knudsen number in the developed current in the microchannel with Ref. [23] for $Re = 0.01$

	$Kn = 0.015$	$Kn = 0.02$	$Kn = 0.03$	$Kn = 0.04$	$Kn = 0.046$
Nu from present work	7.23	7.20	7.09	6.78	6.63
Nu from Ref. [23]	7.42	7.31	7.15	6.80	6.60
$C_f Re$ from present work	21.10	20.81	19.48	18.63	18.01
$C_f Re$ from Ref. [23]	21.49	21.15	19.75	18.85	18.20

Table 3 Thermo-physical properties of FMWCNT/water [45]

mass% FMWNT/water	$\rho/\text{Kg m}^{-3}$	$K/W \text{ m}^{-1} \text{ K}^{-1}$	$\mu/\text{Pa s}$
Pure water	996	0.62	7.65×10^{-4}
Pure water + 0.25% of FMWNT	1008	0.75	7.95×10^{-4}

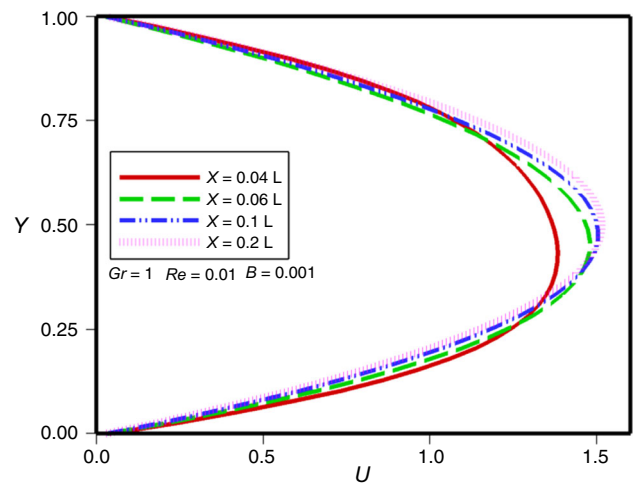


Fig. 5 U profiles at different sections of the microchannel for $B = 0.001$ and $Gr = 1$

In Fig. 5, the flow after the microchannel input tends to development. The maximum velocity U_{max} occurs in the horizontal axis.

In Fig. 6, the velocity profile is displayed for different Gr in different sections. In the rule of forced convective heat transfer ($Gr = 1$), the presence of the slip velocity at $Y = 0$ and $Y = 1$ is well seen in this figure and its maximum value is at the microchannel input which decreases with movement along it and eventually reaches a constant value. Reducing the slip velocity along the microchannel is observed for different values of X . By increasing the Grashof number and generating buoyancy force, the flow moves toward the mixed convection heat transfer. At $Gr = 10$ the effect of gravity on mixed convection causes a change in the velocity profile and a negative slip velocity. The velocity changes are increased at the microchannel input and more movement along the microchannel is needed to reach the developed flow. At $Gr = 10$, the shape of the velocity profile at $X = 0.06 \text{ L}$ and $X = 0.1 \text{ L}$ return flow and the resulting recirculating cell in the range of

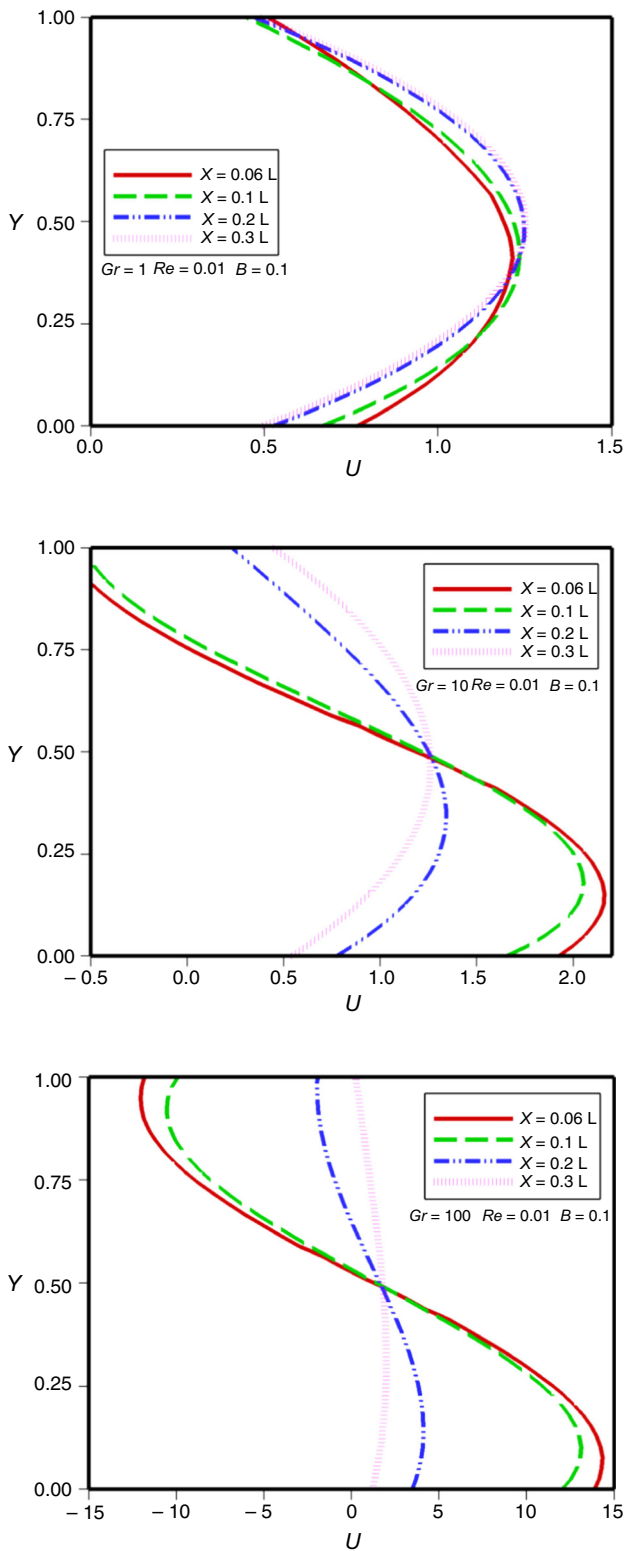


Fig. 6 U profiles at different sections of the microchannel for $B = 0.1$ and $Gr = 1, 10$ and 100

$Y > 0.5$. The buoyancy force is diminished increasing X by moving ahead of the input and the velocity profile approaches the development and symmetrical shape. The

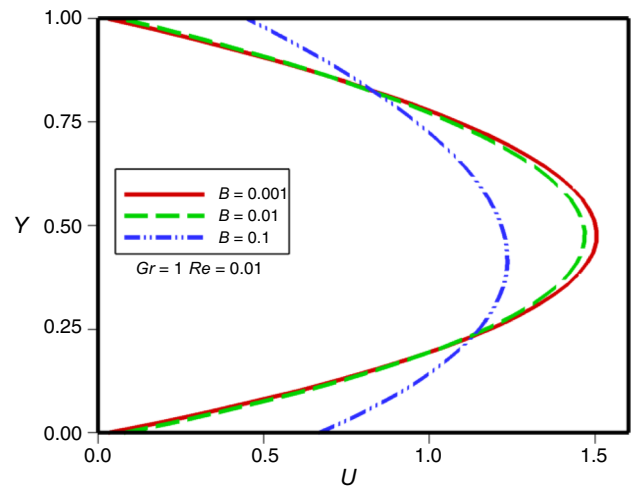


Fig. 7 U Profiles at section $X = 0.1 L$ for different values of slip coefficient

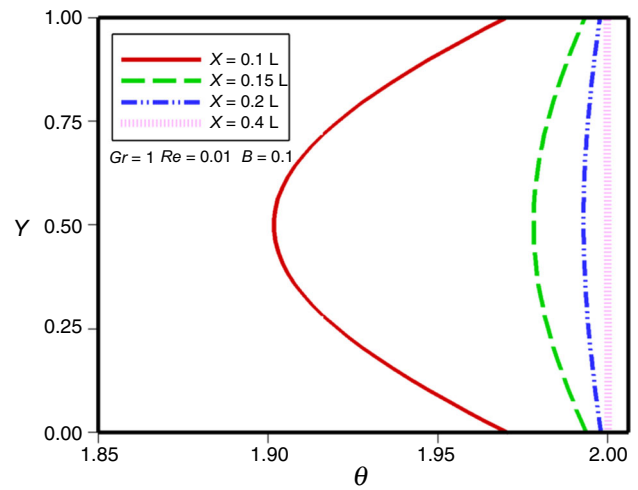


Fig. 8 Profiles of θ at different sections of the microchannel for $B = 0.1$ and $Gr = 1$

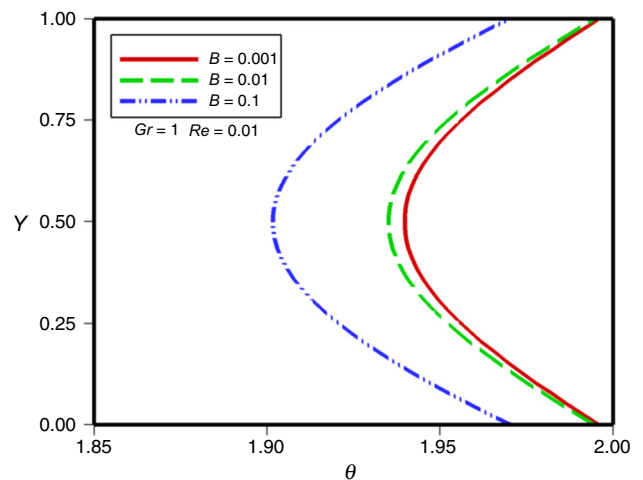
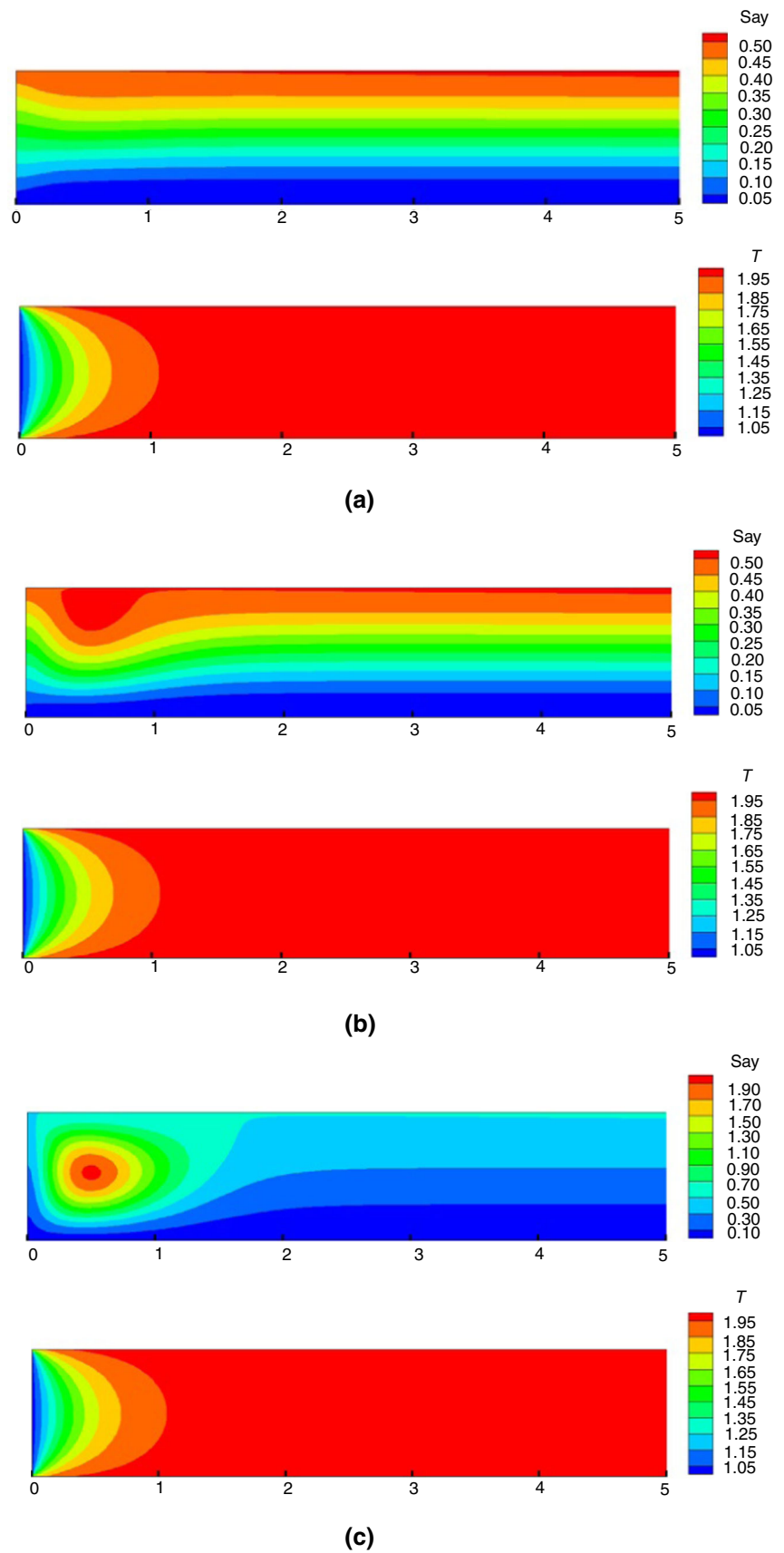


Fig. 9 Profiles of θ at different slip coefficient at $X = 0.1 L$ and $Gr = 1$

Fig. 10 Streamlines and dimensionless isotherms in the microchannel in **a** $Gr = 1$, **b** $Gr = 10$, **c** $Gr = 100$



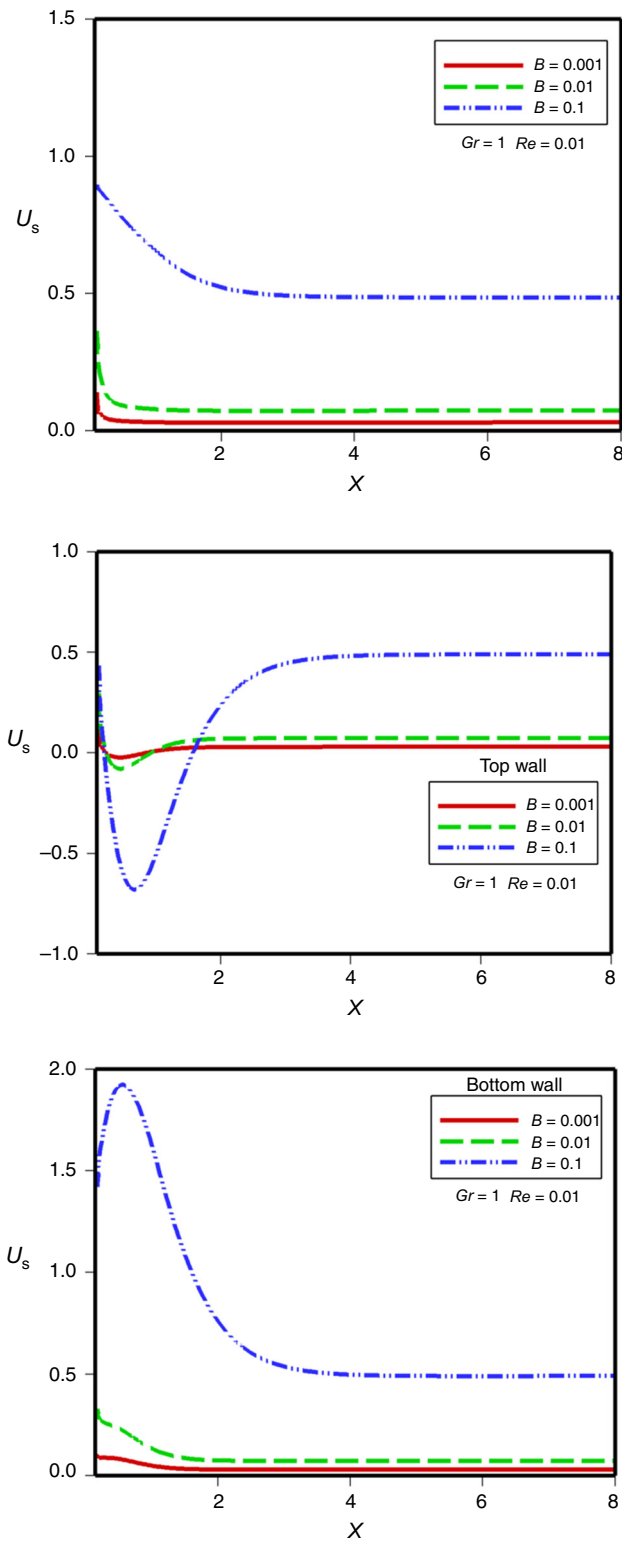


Fig. 11 Changes in U_s for different values of slip coefficient and $Gr = 1, 10$

reason for the presence of a strong buoyancy force at the microchannel input is the difference in temperature between the input fluid and the walls especially in the

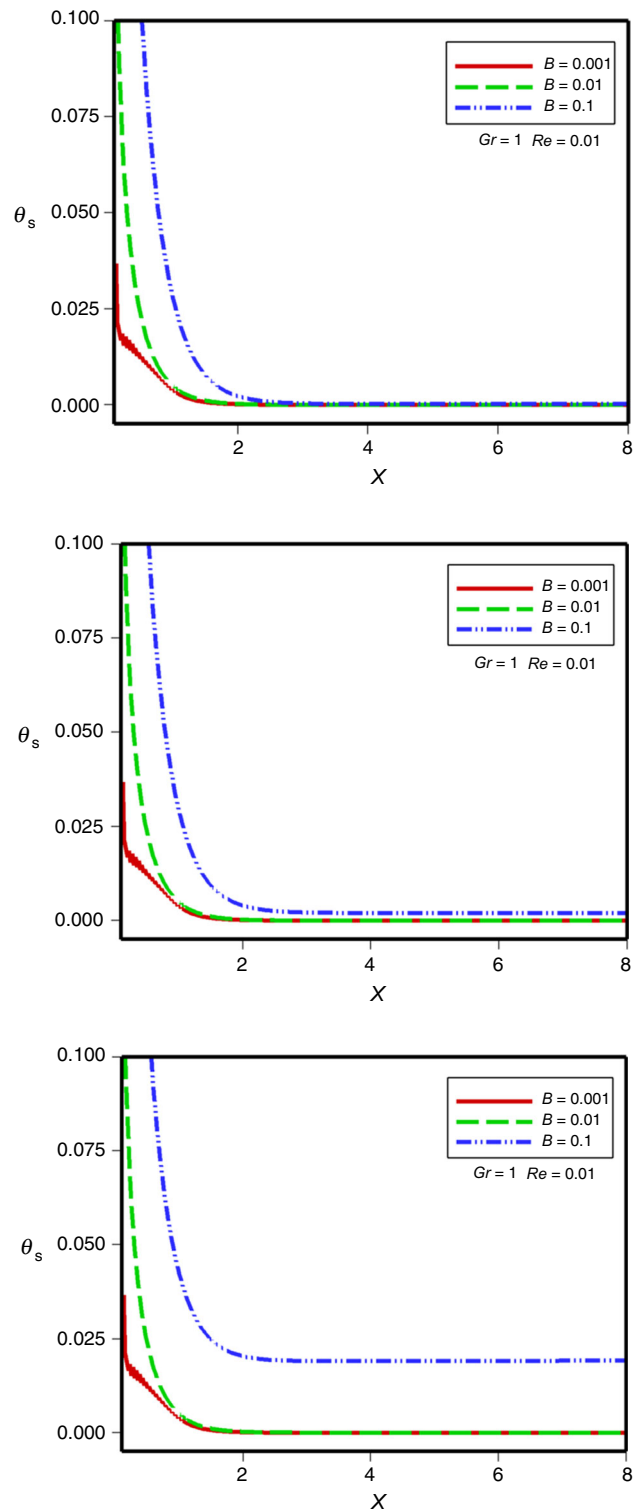


Fig. 12 θ_s along microchannel for different values of slip coefficient in $Gr = 1, 10$ and 100

input. As the fluid moves along the path and the temperature difference between the fluid and the walls is reduced, the free movement force is reduced and the velocity profile develops. This powerful buoyancy force on the upper wall

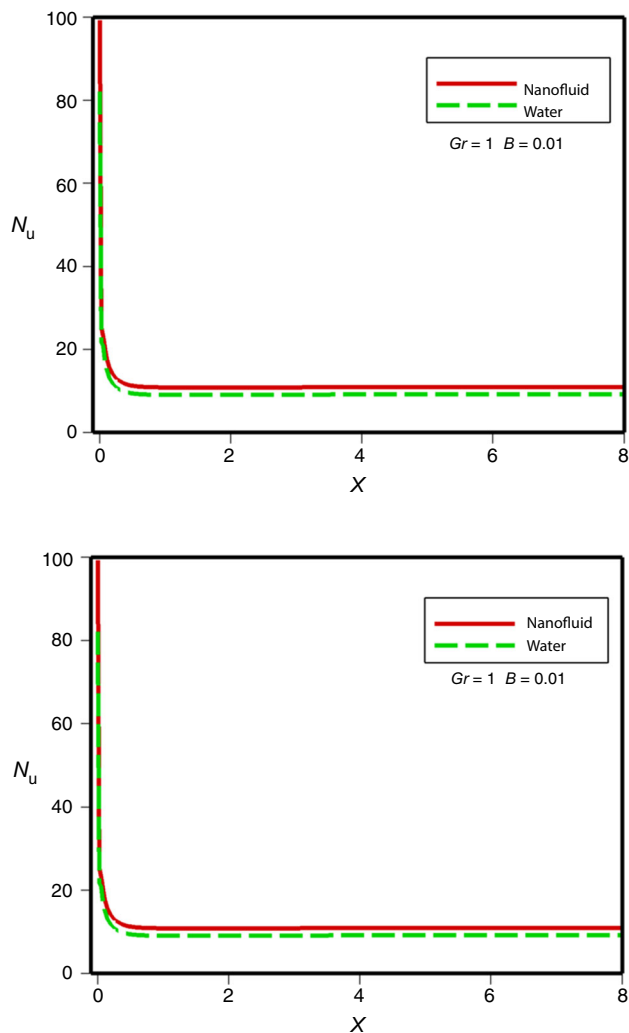


Fig. 13 The variations of Nusselt number along the microchannel walls for nanofluid (*FMWCNT* in water with mass fraction of 0.0025) versus pure water

leads to a negative slip velocity resulting from a return flow in the area. This phenomenon is only due to gravity and the negative value of the velocity profile at $Y > 0.75$. At $Gr = 100$, it can be seen that with the increase in the Grashof number and the stronger buoyancy force, the velocity profile has a higher negative slip rate which can affect the velocity profile at points far from the flow input section. Comparison of Figs. 5 and 6 shows that in the rule of forced convective heat transfer ($Gr = 1$), it is observed that the buoyancy force is diminished by increasing the slip coefficient (B) and separating nanoparticles from each other. Also more B leads to higher value of slip velocity.

Figure 7 shows velocity profile for different values of slip coefficient. In this figure, it is clearly seen that the higher slip coefficient leads to an increase in slip velocity on the walls. Also, by increasing the amount of slip velocity on the walls the maximum velocity decreases in

the horizontal axis of the microchannel. Figure 8 shows the dimensionless temperature profile $\theta = T/T_{in}$ at different sections of the flow. The increase in fluid temperature due to heat exchange with hot walls is evident; therefore the temperature gradient is high at the microchannel input. As the fluid moves along the path and the nanofluid temperature increases, the flow will be convective and this convection is evident at $X = 0.4$ L.

It can be seen from Figs. 6 and 8 that the slip velocity has led to temperature jump which has dropped along the microchannel. Figure 9 shows the dimensionless temperature profile $\theta = T/T_{in}$ for different values of slip coefficient at $X = 0.1$ L. This figure clearly indicates an increase in the amount of temperature jump due to the increase in the slip coefficient. Figure 10a–c presents the streamlines and isotherms for different values of Grashof number in the range of one-sixth of the input from the microchannel length for the sake of clarity. In Fig. 10a, in the flow lines at $Gr = 1$ the flow is developed and exits on the right side after entering the microchannel without changing. In this figure the flow lines are completely parallel and there is no trace of the buoyancy force and the recirculating cell. In Fig. 10b, in $Gr = 10$ by increasing the buoyancy force and creating buoyancy motions, the flow after entering microchannel is dragged down under the influence of gravity and then its temperature is increased through the exchange of heat with the hot walls and, as a result, the buoyancy force pushes it up and creates a weak cell in the input region. Figure 10c shows that the same cell is formed in $Gr = 100$ but due to the strong buoyancy forces a recirculating cell is created in the opposite direction of the input fluid. Since the circulation direction is counter-clockwise, it leads to a negative slip velocity in the input area.

Figure 11 shows the variations in the slip velocity U_s along the microchannel for different values of slip coefficient. In the rule of forced flow convection $Gr = 1$, due to the flow lines and the parallelism of the flow lines, the slip velocities in the upper and lower walls match. Also it is seen that slip velocity has its greatest value at inlet, and then it decreases mildly along the microchannel wall to approach a constant value. For $Gr = 10$, the slip velocity of the input area is obvious in the upper and lower walls which is affected by buoyancy motions. At distances away from the input section the nanofluid temperature tends to the wall temperature and the buoyancy motions due to free movement are weak. It is observed that as the nanofluid moves along the path, the slip velocity decreases and eventually reaches a constant value. The phenomenon of negative slip velocity is evident along the wall for $Gr = 10$ which its amount will be increased with B . In the lower wall for $Gr = 100$ the positive slip velocity increases and then reaches a constant value.

In Fig. 12, the temperature jump (θ_S) changes along the upper wall of the microchannel are shown for different values of slip coefficient. In this figure temperature jump is increased by slip coefficient. For a specific Gr , the temperature jump decreases along the microchannel path so that it reaches the constant value of zero. At $Gr = 100$ where there is a strong buoyancy force, this constant value is slightly greater than zero for $B = 0.1$. Figure 13 shows the variations of Nusselt number along the microchannel walls for nanofluid ($FMWCNT$ in water with mass fraction of 0.0025) versus pure water. The positive effect of adding CNTs to increase Nu of the base fluid can be seen clearly in this figure.

Conclusions

In the present study mixed convection of water/functionalized multi-wall carbon nanotubes ($FMWCNT$) nanofluid flow is simulated in a microchannel with hot walls by the lattice Boltzmann method. Given the gravity in this research and the emergence of buoyancy force the flow velocity components changed and therefore the relationships used to compute macroscopic properties were corrected to include these changes. By increasing the slip coefficient, the slip velocity and temperature jumps also increase. The maximum of these parameters occurred in the input region, and afterward, their amount had a decreasing trend to reach a corresponding constant value along its path. Including the gravity term in Boltzmann equation as an external force changed motion properties and increases the length of the hydrodynamic input length of the flow. Gravity creates powerful buoyancy motions at the input area. Therefore, in the input range where the temperature gradient between the nanofluid and the wall is high, the required distance for flow development increases. For $Gr = 1$ the rule of forced convective heat transfer the buoyancy is negligible and for higher values of Grashof number $Gr = 100$ the buoyancy force creates buoyancy motions in the input region. So that in $Gr = 100$ the vortex power increases and the gravitational buoyancy force changes the hydrodynamic properties of the flow such as the slip velocity and coefficient of friction. These changes lead to the formation of a counterclockwise vortex along the flow direction.

References

1. Nguyen NT, Wereley ST. Fundamentals and applications of microfluidics. 2nd ed. Norwood: Artech house INC; 2006.
2. Fox RW, McDonald AT. Introduction to fluid mechanics. Wiley: New York; 1994.
3. Koplik PJ, Banavar JR. Continuum deductions from molecular hydrodynamic. *Annu Rev Fluid Mech.* 1995;27:257–95.
4. Brid G. Molecular gas dynamics and the direct simulation of gas flows. Oxford: Oxford University Press; 1994.
5. Oran ES, Oh CK, Cybyk BZ. Direct simulation Monte Carlo: recent advances and applications. *Ann Rev Fluid Mech.* 1998;30(1):403–41.
6. Kandlikar S, Garimella S, Li D, Colin S, King MR. Heat transfer and flow in minichannels and microchannels. Amsterdam: Elsevier; 2005.
7. Change CC, Yang TT, Yen TH, Chen COK. Numerical investigation into thermal mixing efficiency in Y-shaped channel using lattice Boltzmann method and field synergy principle. *Int J Therm Sci.* 2009;48(11):2092–9.
8. Wang M, He J, Yu J, Pan N. Lattice Boltzmann modeling of the effective thermal conductivity for fibrous materials. *Int J Therm Sci.* 2007;46(9):848–55.
9. Xuan Y, Li Q, Ye M. Investigations of convective heat transfer in Ferro fluid microflows using lattice-Boltzmann approach. *Int J Therm Sci.* 2007;46(2):105–11.
10. Nie X, Doolen GD, Chen S. Lattice-Boltzmann simulation of fluid flows in MEMS. *J Stat Phys.* 2002;107:279–89.
11. Ho C, Tai Y. Micro-electro-mechanical-systems (MEMS) and fluid flows. *Annu Rev Fluid Mech.* 1998;30:579–612.
12. Gruceliski A, Pozorski J. Lattice Boltzmann simulation of fluid flow in porous media of temperature—affected geometry. *J Theor Appl Mach.* 2012;50:193–214.
13. Kefayati G, Hosseinizadeh S, Gorji M, Sajjadi H. Lattice Boltzmann simulation of natural convection in tall enclosures using water/SiO₂ nanofluid. *Int Commun Heat Mass Transf.* 2011;38:798–805.
14. Yang YT, Lai FH. Numerical study of flow and heat transfer characteristics of alumina-water nanofluids in a microchannel using lattice Boltzmann method. *Int Commun Heat Mass Transf.* 2011;38:607–14.
15. Zhang YH, Qin RS, Sun YH, Barber RW, Emerson DR. Gas flow in microchannels—a lattice Boltzmann method approach. *J Stat Phys.* 2005;121:257–67.
16. Frisch U, Hasslacher B, Pomeau Y. Lattice-gas automata for the Navier–Stokes equation. *Phys Rev.* 1989;56:1505–8.
17. Buick M. Lattice Boltzmann method in interfacial wave modeling. Ph.D. thesis at University of Edinburgh; 1997.
18. He X, Chen S, Doolen GD. A novel thermal model for the lattice Boltzmann method in incompressible limit. *J Comput Phys.* 1998;146:283–300.
19. Guo Z, Shi B, Wang N. Lattice BGK model for incompressible Navier–Stokes equation. *J Comput Phys.* 2000;165(1):288–306.
20. D’Orazio A, Corcione M, Celata GP. Application to natural convection enclosed flows of a lattice Boltzmann BGK model coupled with a general purpose thermal boundary condition. *Int J Therm Sci.* 2004;43(6):575–86.
21. D’Orazio A, Succi S. Simulating two-dimensional thermal channel flows by means of lattice Boltzmann method with new boundary conditions. *Future Gener Comput Syst.* 2004;20:935–44.
22. Karimipour A, Nezhad AH, D’Orazio A, Shirani E. Investigation of the gravity effects on the mixed convection heat transfer in a microchannel using lattice Boltzmann method. *Int J Therm Sci.* 2012;54:142–52.
23. Kavehpour HP, Faghri M. Effect of compressibility and rarefaction on gaseous flow in microchannels. *Numer Heat Transf.* 1997;32:677–96.
24. Chen S, Doolen G. Lattice Boltzmann method for fluid flows. *Annu Rev Fluid Mech.* 1998;30:329–64.

25. Chen S, Tian Z. Simulation of thermal micro-flow using lattice Boltzmann methods with Langmuir slip model. *Int J Heat Fluid Flow*. 2010;31:227–35.
26. Svea O, Skocek J. Simple Navier's slip boundary condition for the non-Newtonian Lattice Boltzmann fluid dynamics solver. *J Non Newton Fluid Mech*. 2013;199:61–9.
27. Monfared AEF, Sarrafi A, Jafari S, Schaffie M. Thermal flux Simulations by lattice Boltzmann method; investigation of high Richardson number cross flows over tandem square cylinders. *Int J Heat Mass Transf*. 2015;86:563–80.
28. Li W, Zhou X, Dong B, Sun T. A thermal LBM model for studding complex flow and heat transfer problems in body-fitted coordinates. *Int J Therm Sci*. 2015;98:266–76.
29. Yu D, Mei R, Lue LS, Shyy Y. Viscous flow computations in the method of lattice Boltzmann equation. *Prog Aerosp Sci*. 2003;39:329–67.
30. Al-Zoubi A, Brenner G. Simulating fluid flow over sinusoidal surfaces using the lattice Boltzmann method. *Comput Math Appl*. 2008;55:1365–76.
31. Breuers M, Bernsdorf J, Zeiser T, Durst F. Accurate computations of the laminar flow past a square cylinder based on two different methods; lattice-Boltzmann and finite-volume. *Int J Heat Fluid Flow*. 2000;21:186–96.
32. Bouzidi M, Humieres DD, Lallemand P, Lue LS. Lattice Boltzmann equation on two-dimensional rectangular grid. *J Comput Phys*. 2001;172:704–17.
33. Rahmati AR, Tahery AA. Numerical study of nanofluid natural convection in a square cavity with a hot obstacle using lattice Boltzmann method. *Alex Eng J*. 2017.
34. Hussain S, Sameh E, Akbar T. Entropy generation analysis in MHD mixed convection of hybrid nanofluid in an open cavity with a horizontal channel containing an adiabatic obstacle. *Int J Heat Mass Transf*. 2017;114(2017):1054–66.
35. Zadkhash M, Toghraie D, Karimipour A. Developing a new correlation to estimate the thermal conductivity of MWCNT-CuO/water hybrid nanofluid via an experimental investigation. *J Therm Anal Calorim*. 2017;129(2):859–67.
36. Arabpour A, Karimipour A, Toghraie D. The study of heat transfer and laminar flow of kerosene/multi-walled carbon nanotubes (MWCNTs) nanofluid in the microchannel heat sink with slip boundary condition. *J Therm Anal Calorim*. 2018;131(2):1553–66.
37. Arabpour A, Karimipour A, Toghraie D, Akbari OA. Investigation into the effects of slip boundary condition on nanofluid flow in a double-layer microchannel. *J Therm Anal Calorim*. 2018;131(3):2975–91.
38. Sheikholeslami M, Sadoughi MK. Mesoscopic method for MHD nanofluid flow inside a porous cavity considering various shapes of nanoparticles. *Int J Heat Mass Transf*. 2017;113:106–14.
39. Lim CY, Shu C, Niu XD, Chew YT. Application of lattice Boltzmann method to simulate microchannel flows. *Phys Fluid*. 2002;14:2299–308.
40. Sofonea V, Sekerka RF. Boundary conditions for the upwind finite difference Lattice Boltzmann model: evidence of slip velocity in micro channel flow. *J Comput Phys*. 2005;207:639–59.
41. Das K, Jana S, Kundu PK. Thermophoretic MHD slip flow over a permeable surface with variable fluid properties. *Alex Eng J*. 2015;54:35–44.
42. Shu C, Niu XD, Chew YT. A Lattice Boltzmann kinetic model for micro flow and heat transfer. *J Stat Phys*. 2005;121:239–55.
43. Liu X, Guo Z. A lattice Boltzmann study of gas flows in a long micro-channel. *Comput Math Appl*. 2013;65:186–93.
44. Yuan Y, Rahman S. Extended application of lattice Boltzmann method to rarefied gas flow in micro-channels. *Phys A*. 2016;463:25–36.
45. Nikkhab Z, Karimipour A, Safaei MR, Forghani-Tehrani P, Goodarzi M, Dahari M, Wongwises S. Forced convective heat transfer of water/functionalized multi-wall carbon nanotube nanofluids in a microchannel with oscillating heat flux and slip boundary condition. *Int Commun Heat Mass Transf*. 2015;68:69–77.
46. Alamyane AA, Mohammad AA. Simulation of forced c convection in channel with extend surface by the lattice Boltzmann method. *Comput Math Appl*. 2010;59:241–2430.
47. Verhaeghe F, Luo LS, Blanpain B. Lattice Boltzmann modeling of microchannel flow in slip flow regime. *J Comput Phys*. 2009;10:147–57.
48. Zou Q, He X. on pressure and velocity flow boundary conditions and bounce back for the lattice Boltzmann BGK model. *Comp Gas*. 1996;1:961–1001.
49. Dorazio A, Arrighetti C, Succi S. Kinetic scheme for fluid flows with heat transfer. Ph.D. thesis, La Spaienza: University of Rom; 2003.
50. Deghani Y, Abdollahi A, Karimipour A. Experimental investigation toward obtaining a new correlation for viscosity of WO_3 and Al_2O_3 nanoparticles-loaded nanofluid within aqueous and non-aqueous basefluids. *J Therm Anal Calorim*. <https://doi.org/10.1007/s10973-018-7394-5>.
51. Hassani M, Karimipour A. Discrete ordinates simulation of radiative participating nanofluid natural convection in an enclosure. *J Therm Anal Calorim*: 1–13.
52. Karimipour A, Nezhad AH, D'Orazio A, Esfe MH, Safaei MR, Shirani E. Simulation of copper-water nanofluid in a microchannel in slip flow regime using the lattice Boltzmann method. *Eur J Mech B Fluids*. 2015;49:89–99.
53. Karimipour A, Nezhad AH, D'Orazio A, Shirani E. The effects of inclination angle and Prandtl number on the mixed convection in the inclined lid driven cavity using lattice Boltzmann method. *J Theor Appl Mech*. 2013;51(2):447–62.
54. Afrand M, Rostami S, Akbari M, Wongwises S, Esfe MH, Karimipour A. Effect of induced electric field on magneto-natural convection in a vertical cylindrical annulus filled with liquid potassium. *Int J Heat Mass Transf*. 2015;90:418–26.
55. Bahrami M, Akbari M, Karimipour A, Afrand M. An experimental study on rheological behavior of hybrid nanofluids made of iron and copper oxide in a binary mixture of water and ethylene glycol: non-Newtonian behavior. *Exp Therm Fluid Sci*. 2016;79:231–7.
56. Esfe MH, Arani AAA, Karimiopour A, Esforjani SSM. Numerical simulation of natural convection around an obstacle placed in an enclosure filled with different types of nanofluids. *Heat Transf Res*. 2014;45(3):279–92.
57. Mahmoodi M, Esfe MH, Akbari M, Karimipour A, Afrand M. Magneto-natural convection in square cavities with a source-sink pair on different walls. *Int J Appl Electromagn Mech*. 2015;47(1):21–32.
58. Esfandiary M, Mehmandoust B, Karimipour A, Pakravan HA. Natural convection of Al_2O_3 -water nanofluid in an inclined enclosure with the effects of slip velocity mechanisms: Brownian motion and thermophoresis phenomenon. *Int J Therm Sci*. 2016;105:137–58.
59. Karimipour A, D'Orazio A, Shadloo MS. The effects of different nano particles of Al_2O_3 and Ag on the MHD nano fluid flow and heat transfer in a microchannel including slip velocity and temperature jump. *Phys E*. 2017;86:146–53.
60. Goodarzi M, Safaei MR, Oztop HF, Karimipour A, Sadeghinezhad E, Dahari M, Kazi SN, Jomhari N. Numerical study of entropy generation due to coupled laminar and turbulent mixed convection and thermal radiation in an enclosure filled with a semitransparent medium. *Sci World J*. 2014;2014:761745.

61. Toghianiyan A, Zarringhalam M, Akbari OA, Sheikh Shabani GA, Toghraie D. Application of lattice Boltzmann method and spinodal decomposition phenomenon for simulating two-phase thermal flows. *Phys A*. 2018;509:673–89.
62. Jourabian M, Darzi AAR, Toghraie D, Ali Akbari O. Melting process in porous media around two hot cylinders: numerical study using the lattice Boltzmann method. *Phys A*. 2018;509:316–35.
63. Nemati M, Abady ARSN, Toghraie D, Karimipour A. Numerical investigation of the pseudopotential lattice Boltzmann modeling of liquid–vapor for multi-phase flows. *Phys A*. 2018;489:65–77.
64. Tohidi M, Toghraie D. The effect of geometrical parameters, roughness and the number of nanoparticles on the self-diffusion coefficient in Couette flow in a nanochannel by using of molecular dynamics simulation. *Phys B*. 2017;518:20–32.
65. Toghraie D, Mokhtari M, Afrand M. Molecular dynamic simulation of copper and platinum nanoparticles Poiseuille flow in a nanochannels. *Phys E*. 2016;84:152–61.
66. Rezaei M, Azimian AR, Toghraie D. Molecular dynamics study of an electro-kinetic fluid transport in a charged nanochannel based on the role of the stern layer. *Phys A*. 2015;426:25–34.
67. Rezaei M, Azimian AR, Semiromi DT. The surface charge density effect on the electro-osmotic flow in a nanochannel: a molecular dynamics study. *Heat Mass Transf*. 2015;51(5):661–70.
68. Karimipour A, Esfe MH, Safaei MR, Semiromi DT, Jafari S, Kazi SN. Mixed convection of copper–water nanofluid in a shallow inclined lid driven cavity using the lattice Boltzmann method. *Phys A*. 2014;402:150–68.
69. Semiromi DT, Azimian AR. Molecular dynamics simulation of nonodroplets with the modified Lennard-Jones potential function. *Heat Mass Transf*. 2011;47(5):579–88.
70. Noorian H, Toghraie D, Azimian AR. The effects of surface roughness geometry of flow undergoing Poiseuille flow by molecular dynamics simulation. *Heat Mass Transf*. 2014;50(1):95–104.
71. Shamsi MR, Akbari OA, Marzban A, Toghraie D, Mashayekhi R. Increasing heat transfer of non-Newtonian nanofluid in rectangular microchannel with triangular ribs. *Phys E*. 2017;93:167–78.
72. Esfe MH, Rostamian H, Toghraie D, Yan WM. Using artificial neural network to predict thermal conductivity of ethylene glycol with alumina nanoparticle. *J Therm Anal Calorim*. 2016;126(2):643–8.
73. Semiromi DT, Azimian AR. Molecular dynamics simulation of annular flow boiling with the modified Lennard-Jones potential function. *Heat Mass Transf*. 2012;48(1):141–52.
74. Nazari M, Mohebbi R, Kayhani MH. Power-law fluid flow and heat transfer in a channel with a built-in porous square cylinder: lattice Boltzmann simulation. *J Non Newton Fluid Mech*. 2014;204:38–49.
75. Nazari M, Kayhani MH, Mohebbi R. Heat transfer enhancement in a channel partially filled with a porous block: lattice Boltzmann method. *Int J Mod Phys C*. 2013;24(09):1350060.
76. Mohebbi R, Nazari M, Kayhani MH. Comparative study of forced convection of a power-law fluid in a channel with a built-in square cylinder. *J Appl Mech Tech Phys*. 2016;57(1):55–68.
77. Mohebbi R, Rashidi MM. Numerical simulation of natural convection heat transfer of a nanofluid in an L-shaped enclosure with a heating obstacle. *J Taiwan Inst Chem Eng*. 2017;72:70–84.
78. Mohebbi R, Izadi M, Chamkha AJ. Heat source location and natural convection in a C-shaped enclosure saturated by a nanofluid. *Phys Fluids*. 2017;29(12):122009.
79. Mohebbi R, Heidari H. Lattice Boltzmann simulation of fluid flow and heat transfer in a parallel-plate channel with transverse rectangular cavities. *Int J Mod Phys C*. 2017;28(03):1750042.
80. Ma Y, Mohebbi R, Rashidi MM, Yang Z. Numerical simulation of flow over a square cylinder with upstream and downstream circular bar using lattice Boltzmann method. *Int J Mod Phys C*. 2018;29(04):1850030.
81. Ma Y, Mohebbi R, Rashidi MM, Yang Z. Study of nanofluid forced convection heat transfer in a bent channel by means of lattice Boltzmann method. *Phys Fluids*. 2018;30(3):032001.
82. Ma Y, Mohebbi R, Rashidi MM, Manca O, Yang Z. Numerical investigation of MHD effects on nanofluid heat transfer in a baffled U-shaped enclosure using lattice Boltzmann method. *J Therm Anal Calorim*. 2018. <https://doi.org/10.1007/s10973-018-7518-y>.
83. Ma Y, Mohebbi R, Rashidi MM, Yang Z. Simulation of nanofluid natural convection in a U-shaped cavity equipped by a heating obstacle: effect of cavity's aspect ratio. *J Taiwan Inst Chem Eng*. 2018. <https://doi.org/10.1016/j.jtice.2018.07.026>.
84. Mohebbi R, Lakzayi H, Sidik NAC, Japar WMAA. Lattice Boltzmann method based study of the heat transfer augmentation associated with Cu/water nanofluid in a channel with surface mounted blocks. *Int J Heat Mass Transf*. 2018;117:425–35.
85. Mohebbi R, Rashidi MM, Izadi M, Sidik NAC, Xian HW. Forced convection of nanofluids in an extended surfaces channel using lattice Boltzmann method. *Int J Heat Mass Transf*. 2018;117:1291–303.
86. Izadi M, Mohebbi R, Karimi D, Sheremet MA. Numerical simulation of natural convection heat transfer inside a⁺ shaped cavity filled by a MWCNT-Fe₃O₄/water hybrid nanofluids using LBM. *Chem Eng Process Process Intensif*. 2018;125:56–66.
87. Abchouyeh MA, Mohebbi R, Fard OS. Lattice Boltzmann simulation of nanofluid natural convection heat transfer in a channel with a sinusoidal obstacle. *Int J Mod Phys C*. 2018;29(09):1850079.
88. Mohebbi R, Izadi M, Amiri Delouei A, Sajjadi H. Effect of MWCNT-Fe₃O₄/water hybrid nanofluid on the thermal performance of ribbed channel with apart sections of heating and cooling. *J Therm Anal Calorim*. 2018. <https://doi.org/10.1007/s10973-018-7483-5>.